Supplement of Earth Surf. Dynam., 14, 361–389, 2026
https://doi.org/10.5194/esurf-14-361-2026-supplement

Earth Surface Dynamics
Open Access
EGU

Supplement of

First Alps-wide reconstruction of LGM glacial sediment transport enabled by GPU-accelerated particle tracking

Tancrède P. M. Leger et al.

Correspondence to: Tancrède P. M. Leger (tancrede.leger@unil.ch)

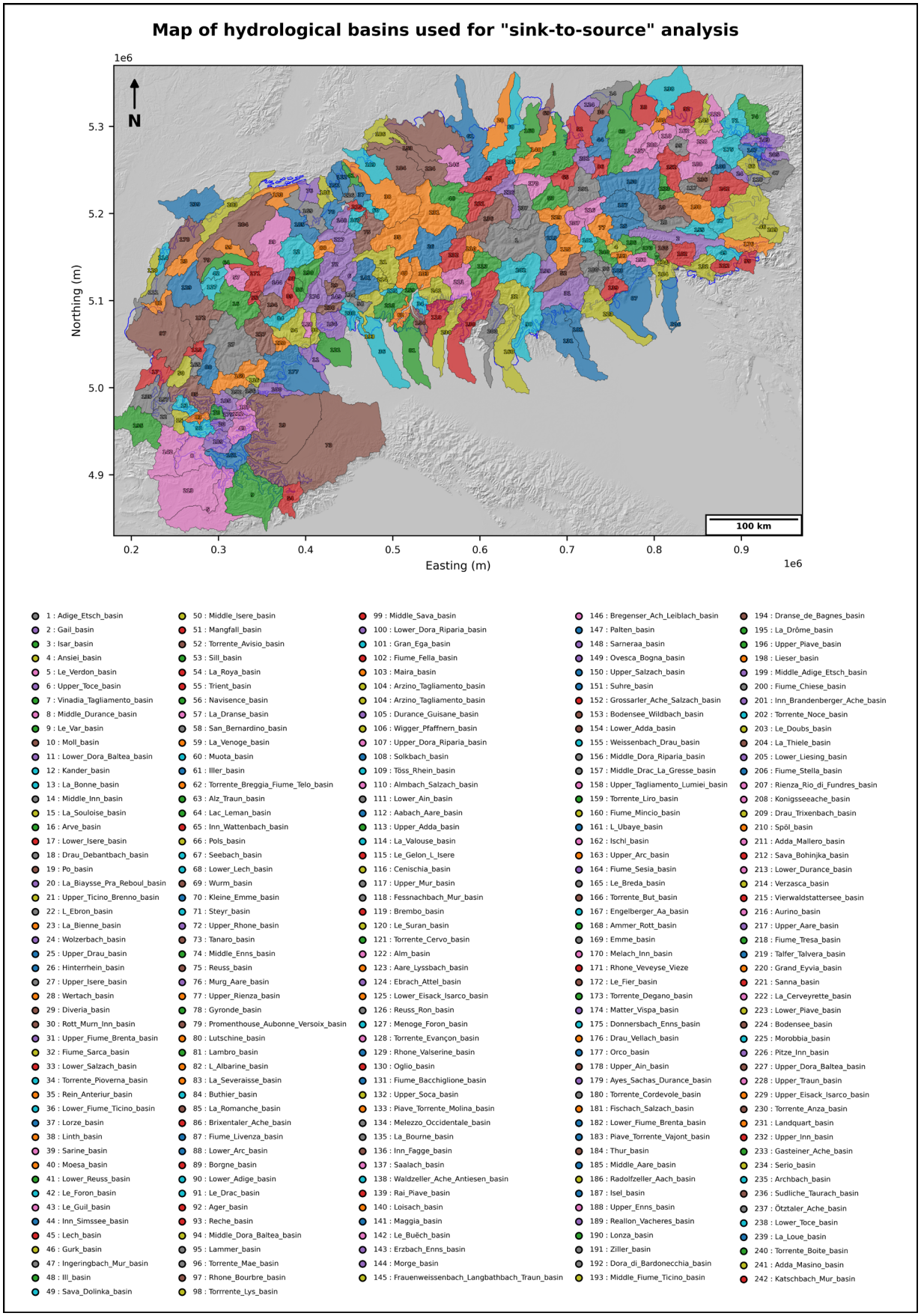

Figure S1. Map and naming convention for all hydrological catchments (n = 242) used to divide our domain into sections and thus quantify the different provenance fractions of modelled ice-contact deposits within our sink-to-source analysis. The hydrological basins were obtained from the global HydroBASINS database (Lehner & Grill, 2013), using a combination of watershed product levels 8 and 9 (more details in Lehner & Grill, 2013).

Table S1. Model-data comparison assessing the agreement between source-to-sink trajectories of specific Alpine surface lithologies versus TCN-dated erratic boulders.

Erratic lithology	Reference	Sample name	Latitude (dd)	Longitude (dd)	Elevation (m a.s.l.)	Exposure age (+/- external uncertainties, yr BP) *	Overlap with modelled trajectories ? ** Complex seeding (subglacial & supraglacial schemes)	Overlap with modelled trajectories ? ** 'Simple' seeding scheme only
Central Aar granite	Reber et al. (2014)	Reuss-21	47.3952	8.1947	446	22030 +/- 1410	Yes (only by Central Aar granites)	Yes (only by Central Aar granites)
Central Aar granite	Reber et al. (2014)	Reuss-22	47.3955	8.1883	475	22270 +/- 1500	Yes (only by Central Aar granites)	Yes (only by Central Aar granites)
Amphibolite	Kamleitner et al. (2023)	Reuss43	47.3957	8.2698	536	18886 +/- 3627	Yes (by Hercynian amphibolites and other lithologies)	No, closest trajectories are 2.2 km away
Arolla Gneiss	Graf et al. (2015)	GRI-1	47.0646	6.8392	1090	22640 +/- 1720	No, closest trajectories are 6 km away (central Aar granite)	No, closest trajectories are 6 km away (central Aar granite)
Central Gneiss	Bichler et al. (2016)	SON2	47.0564	12.9805	2229	18910 +/- 2860	Yes	Yes
Central Gneiss	Bichler et al. (2016)	DUR2	47.0758	12.9834	1643	26380 +/- 3250	Yes	No, closest trajectories are 2.3 km away
Granite	Boxleitner et al. (2019)	Wassen4	46.7080	8.6030	904	18300 +/- 1310	Yes (only by Central Aar granites)	Yes (only by Central Aar granites)
Granite	Gianotti et al. (2008)	Ivrea1	45.4940	7.8790	325	20430 +/- 3280	Yes (only by Mt. Blanc granites)	Yes (only by Mt. Blanc granites)
Granite	Gianotti et al. (2008)	Ivrea6	45.4810	7.8830	317	24240 +/- 2130	Yes (only by Mt. Blanc granites)	Yes (only by Mt. Blanc granites)
Granite	Ivy-Ochs et al. (2018)	SM4	45.0928	7.2815	821	19360 +/- 2190	No, there is no mapped granite outcrops anywhere near this valley and glacier catchment in Italian geological maps used within this study.	No, there is no mapped granite outcrops anywhere near this valley and glacier catchment in Italian geological maps used within this study.
Granite	Kamleitner et al. (2023)	Reuss45	47.4358	8.3074	531	18230 +/- 1360	Yes (only by Central Aar granites)	Yes (only by Central Aar granites)
Granite	Kamleitner et al. (2023)	Reuss40	47.3959	8.2300	473	20250 +/- 1620	Yes (only by Central Aar granites)	Yes (only by Central Aar granites)
Granite	Kamleitner et al. (2023)	Reuss46	47.4406	8.3035	546	21660 +/- 1590	Yes (only by Central Aar granites)	Yes (only by Central Aar granites)
Granite	Prud'homme et al. (2020)	VAU12_B1_06	45.9093	6.76412	1037	23050 +/- 2120	Yes (only by Mt. Blanc granites)	Yes (only by Mt. Blanc granites)
Granite	Roattino et al. (2023)	MIR20-02	45.4550	5.6935	788	23260 +/- 1460	Yes (only by Belledonne granites)	No, closest trajectories are 7.6 km away (Belledone granites)
Granite	Kamleitner et al. (2022)	VR14	45.8518	8.5048	818	18000 +/- 1600	No but trajectories are within 3 km (modelled LGM not extensive enough), only by Central Aar granites	No but trajectories are within 3 km (modelled LGM not extensive enough), only by Central Aar granites
Granite	Braakhekke et al. (2020)	Briallo33	45.7780	8.3790	517	24020 +/- 2960	No but yes with Arolla Gneiss	No
Granite	Kamleitner et al. (2023)	Reuss35	47.3738	8.2713	548	19110 +/- 1220	Yes (only by Central Aar granites)	Yes (only by Central Aar granites)
Granite	Kamleitner et al. (2023)	Reuss39	47.3449	8.3139	460	20750 +/- 1660	Yes (only by Central Aar granites)	Yes (only by Central Aar granites)
Granite	Kamleitner et al. (2023)	Reuss30	47.4493	8.2785	435	21130 +/- 1380	Yes (only by Central Aar granites)	Yes (only by Central Aar granites)
Granite	Kamleitner et al. (2022)	VR43	45.8437	8.5065	764	21710 +/- 1320	No but trajectories are within 3 km (modelled LGM not extensive enough), only by Central Aar granites	No but trajectories are within 3.5 km (modelled LGM not extensive enough), only by Central Aar granites
Granite	Kamleitner et al. (2022)	VR29	45.8448	8.5049	805	23180 +/- 1370	No but trajectories are within 3 km (modelled LGM not extensive enough), only by Central Aar granites	No but trajectories are within 3.5 km (modelled LGM not extensive enough), only by Central Aar granites
Granite	Kamleitner et al. (2022)	VR28	45.8455	8.5048	805	23500 +/- 1370	No but trajectories are within 3 km (modelled LGM not extensive enough), only by Central Aar granites	No but trajectories are within 3.5 km (modelled LGM not extensive enough), only by Central Aar granites
Granite	Kamleitner et al. (2022)	VR44	45.8452	8.5058	797	29550 +/- 1720	No but trajectories are within 3 km (modelled LGM not extensive enough), only by Central Aar granites	No but trajectories are within 3.5 km (modelled LGM not extensive enough), only by Central Aar granites
Granite	Reber et al. (2014)	Reuss-20	47.3476	8.3144	502	18630 +/- 1300	Yes (only by Central Aar granites)	Yes (only by Central Aar granites)
Granite	Wüthrich et al. (2018)	BS6	46.9400	7.5305	762	18220 +/- 1020	Yes (only by Central Aar granites)	Yes (only by Central Aar granites)
Granite	Wüthrich et al. (2018)	BS2	46.8859	7.4886	729	18760 +/- 1700	Yes (only by Central Aar granites)	Yes (only by Central Aar granites)
Granite	Wüthrich et al. (2018)	GS3	46.8515	7.4744	937	19560 +/- 1330	Yes (only by Central Aar granites)	Yes (only by Central Aar granites)
Granite	Wüthrich et al. (2018)	GS1	46.8664	7.4716	873	20410 +/- 1980	Yes (only by Central Aar granites)	Yes (only by Central Aar granites)
Hornblende granite	Ivy-Ochs et al. (2004)	ER7	47.1400	7.6800	610	19850 +/- 1720	Yes (only by Central Aar granites)	Yes (only by Central Aar granites)
Hornblende granite	Ivy-Ochs et al. (2004)	ER1	47.1592	7.6868	580	23920 +/- 1900	Yes (by Central Aar and Mt. Blanc granites)	Yes (only by Central Aar granites)
Hornblende granite	Ivy-Ochs et al. (2004)	ER2	47.1586	7.6828	585	24030 +/- 1630	Yes (by Central Aar and Mt. Blanc granites)	Yes (only by Central Aar granites)
Mt. Blanc Granite	Graf et al. (2015)	PBOL-1	46.7803	6.4891	1190	20990 +/- 1670	Yes: overlap with Central Aar granites trajectories which are undifferentiable (Mt. Blanc granite trajectories are within 5 km)	No but trajectories are within 2 km (only by Central Aar granites though)
Mt. Blanc Granite	Graf et al. (2015)	PAB-1	47.0037	6.9104	710	21360 +/- 1650	Yes: overlap with Central Aar granites trajectories which are undifferentiable (Mt. Blanc granite trajectories are within 1.6 km)	Yes: overlap with Central Aar granites trajectories which are undifferentiable
Mt. Blanc Granite	Graf et al. (2015)	VDR-1	47.0893	6.9645	990	31840 +/- 3040	No, closest trajectories are 5 km away (central Aar granite)	No, closest trajectories are 6 km away (central Aar granite)
Serpentinite	Kamleitner et al. (2022)	VR52	45.6907	8.5763	326	25266 +/- 4135	No, closest serpentinite trajectories are 16 km away	No, closest serpentinite trajectories are 16 km away
Serpentinite	Kamleitner et al. (2022)	VR33	45.7963	8.5021	612	26200 +/- 6832	No, closest serpentinite trajectories are 8 km away	No, closest serpentinite trajectories are 8 km away
Serpentinite	Kamleitner et al. (2022)	VR51	45.7069	8.5311	336	27815 +/- 8677	No, closest serpentinite trajectories are 12 km away	No, closest serpentinite trajectories are 11.5 km away
Summary (complex seeding)	**Model-data fit: 26/38 ~68%**	**Model-data fit would be obtained with small (<4 km) improvement in extent: 5/38 ~13%**				**No model-data fit: 7/38 ~18%**		
Summary (simple seeding)	**Model-data fit: 22/38 ~58%**	**Model-data fit would be obtained with small (<4 km) improvement in extent: 6/38 ~16%**				**No model-data fit: 10/38 ~26%**		

* All exposure ages were re-calculated as part of the compilation of geochronological data for the AlpIce database (Kamleitner *et al*., in prep).

** An overlap between the dated erratic and modelled particle trajectories is defined as such when trajectories of the matching lithology are within a 1 km radius of the erratic location.

Note: only erratic boulders that were dated to between 40 and 18 ka (the time frame of our simulations), and published in peer-reviewed journals, were compiled. Moreover, duplicate samples (with identical or close-by coordinates) were removed. We only keep one sample per study site.

Alps-wide map of source-to-sink particle trajectories (per lithology)

Subglacial seeding

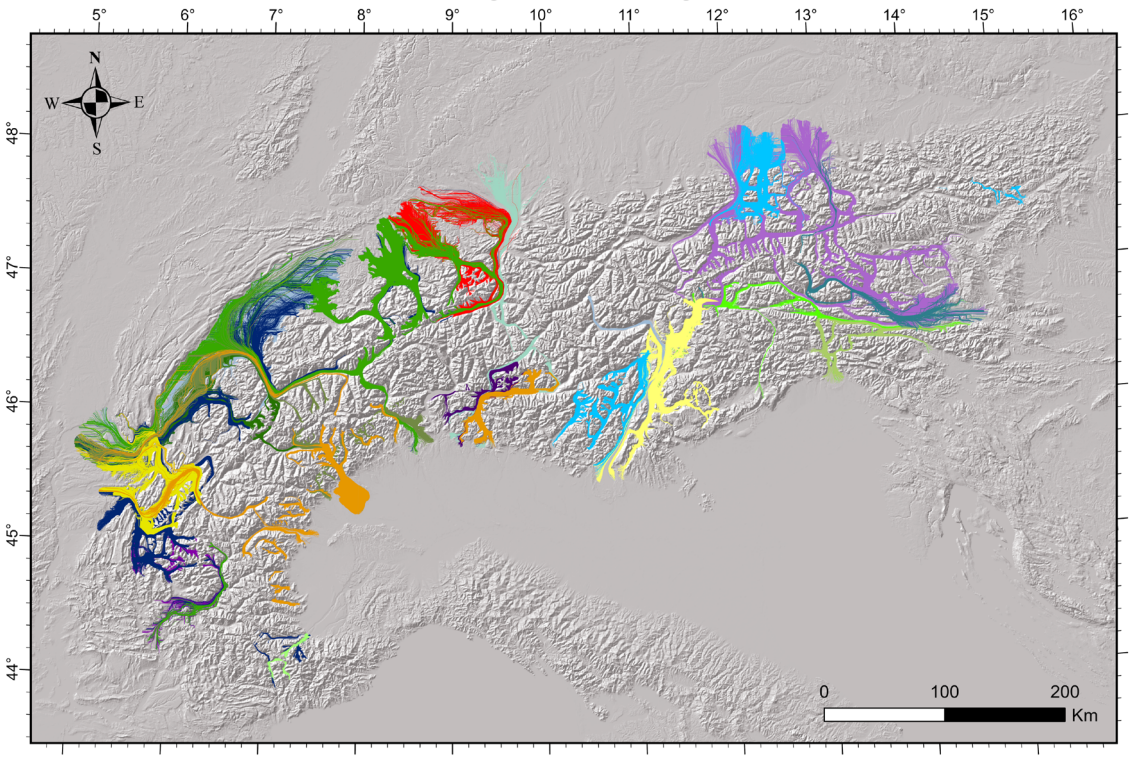

Supraglacial seeding

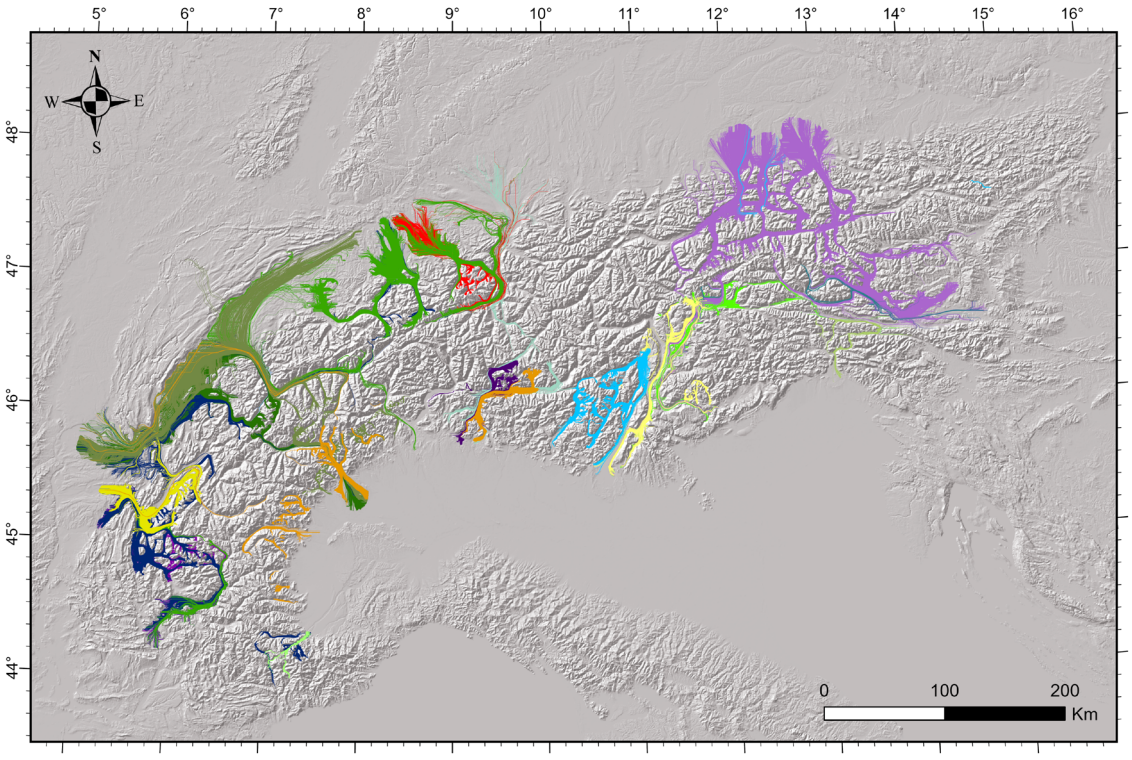

1 : Adamello_tonalite
2 : Antigorite_serpentinite
3 : Argentera_granites
4 : Arolla_gneiss
5 : Belledonne_granites
6 : Bergell_intrusion
7 : Brixen_granite
8 : Central_Aar_granite
9 : Combeynot_pink-green_granite
10 : Eclogite-facies_Allalin_Gabbro
11 : Glarus_Verrucano
12 : Glockner_serpentinites
13 : Grauwackenzone_porphyroids
14 : Hercynian_amphibolites_&_amphibole-rich_gneisses
15 : Hochwipfel_formation
16 : Julier_granites
17 : Mont-Blanc_Granite
18 : Nauders_serpentinite
19 : Oisans_Pelvoux_granites
20 : Salvan-Dorénaz_conglomerate
21 : Tauern_window_Central_Gneiss
22 : Vedrette-di-Ries_tonalite

Figure S2. Map of all source-to-sink particle trajectories produced for each of the 22 surface rock lithologies selected and mapped as part of the source-to-sink analysis, and for both subglacial and supraglacial particle seeding simulations. The trajectories are color-coded according to the lithologies as indicated by the legend. A map indicating the locations of the source polygons (outcrops) for each lithology is shown in the main paper figure 5. In the above maps, overlapping trajectories are vertically ordered following the same alphabetical order presented in the legend. More precise, high-resolution and more zoomed-in maps showing the pathways of particle trajectories for each of these sources are provided in the source-to-sink catalogue provided in the Zenodo repository associated with this paper: https://doi.org/10.5281/zenodo.18374156.

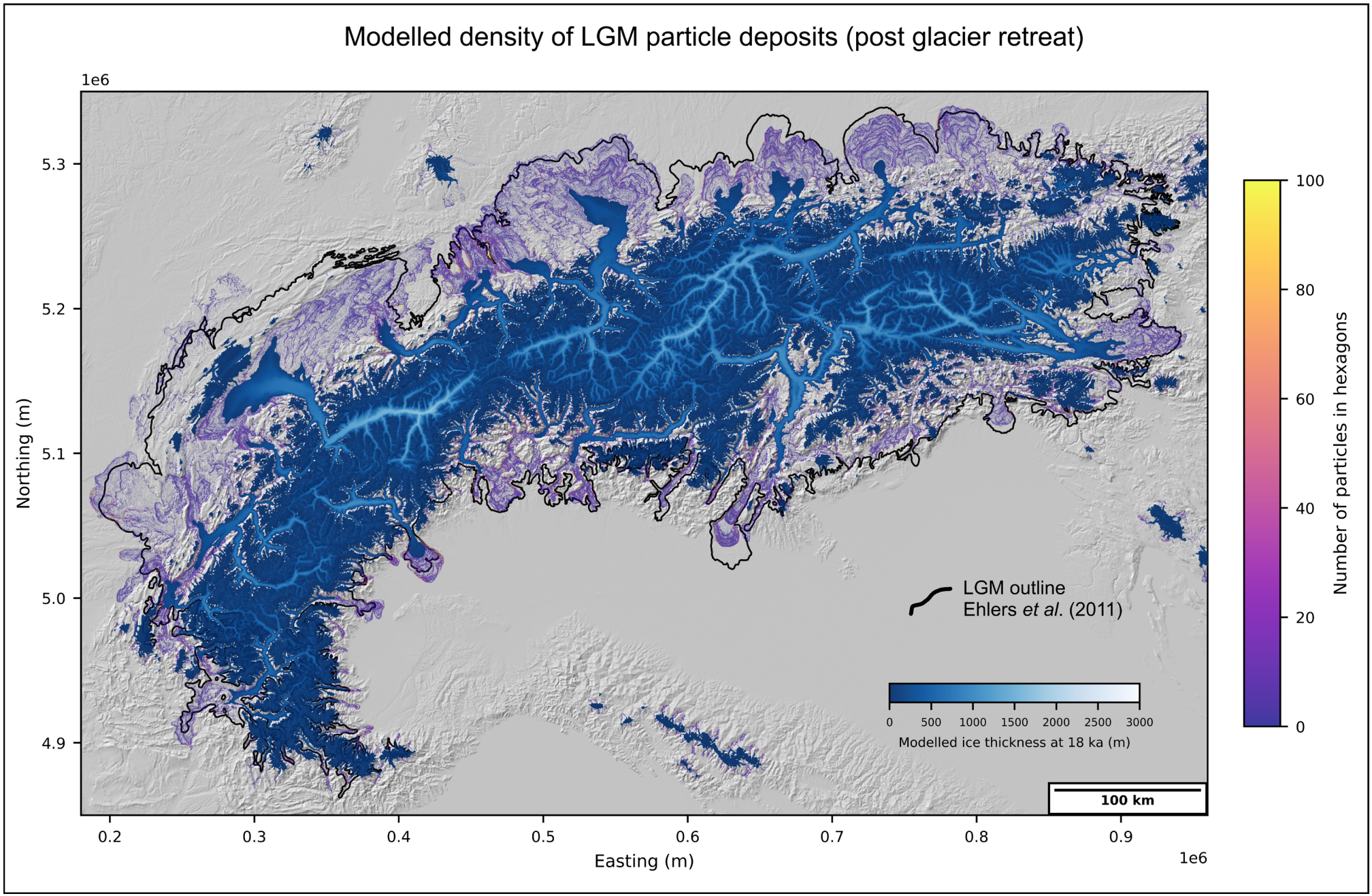
Modelled density of LGM particle deposits (post glacier retreat)
1e6
5.3
5.2
5.1
5.0
4.9
Northing (m)
0.2
0.3
0.4
0.5
0.6
0.7
0.8
0.9
1e6
Easting (m)
LGM outline
Ehlers et al. (2011)
0
500
1000
1500
2000
2500
3000
Modelled ice thickness at 18 ka (m)
100 km
100
80
60
40
20
0
Number of particles in hexagons

Figure S3. Map of modelled particle deposit densities at 18 ka, the final timestep of our AIF simulations of the LGM (40-18 ka), for our entire model domain. The AIF model output is displayed using modelled ice thickness at 18 ka. The particle deposit data shown here combines both datasets of particles seeded subglacially and supraglacially and is expressed in the form of a spatial density map. Each coloured dot is a small hexagon in which the total number of deposited particles is computed. Bright yellow colors indicate hexagons holding the highest concentrations of particles. This model output clearly highlights periods of glacier advances and/or margin stabilization during our AIF model simulations with IGM by forming moraine-like shapes. We argue the novel ability to produce this data over such spatio-temporal scale with Lagrangian particle tracking coupled with glacier evolution modelling opens the door to future model-data comparisons that directly quantify the fit between modelled particle deposits and the preserved glacio-geomorphological record (see Discussion section). This figure caption is also relevant to subsequent Supplementary figures 4-6.

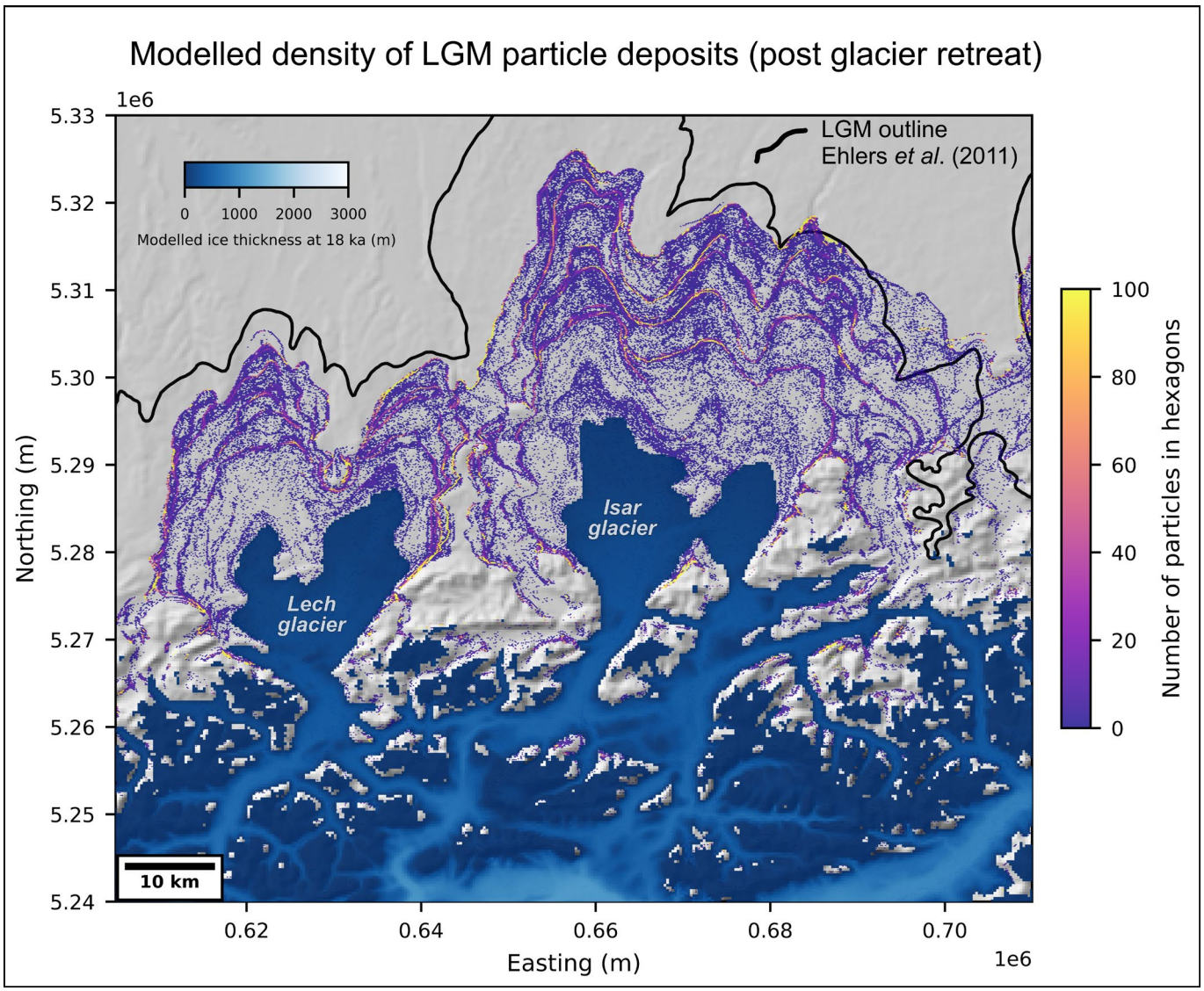

Figure S4. Map of modelled particle deposit densities at 18 ka, the final timestep of our AIF simulations of the LGM (40-18 ka), in the foreland region of the Isar outlet glacier. See Figure S3 for the full figure caption.

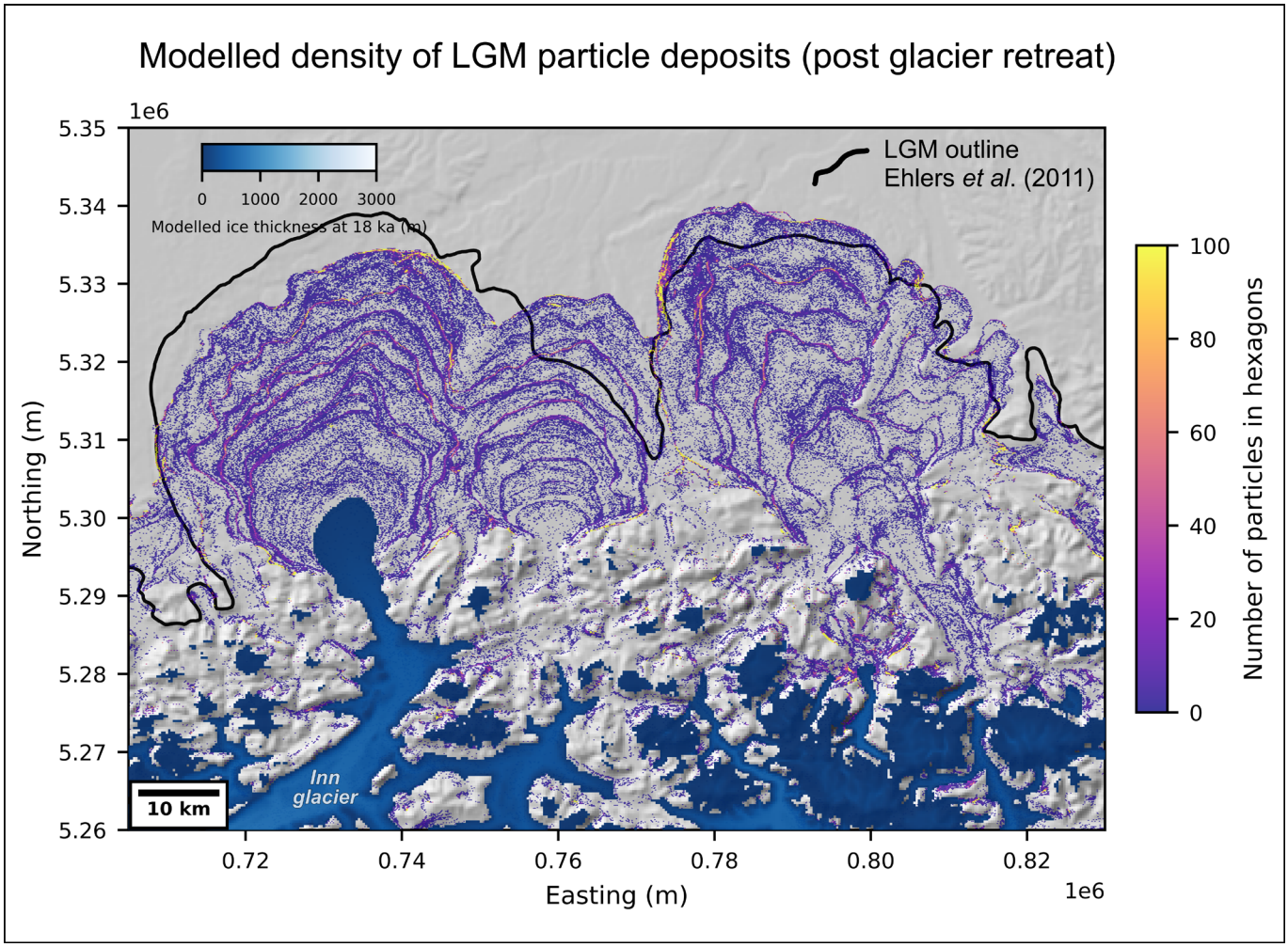

Figure S5. Map of modelled particle deposit densities at 18 ka, the final timestep of our AIF simulations of the LGM (40-18 ka), in the foreland region of the Inn and Salzach outlet glaciers. See Figure S3 for the full figure caption.

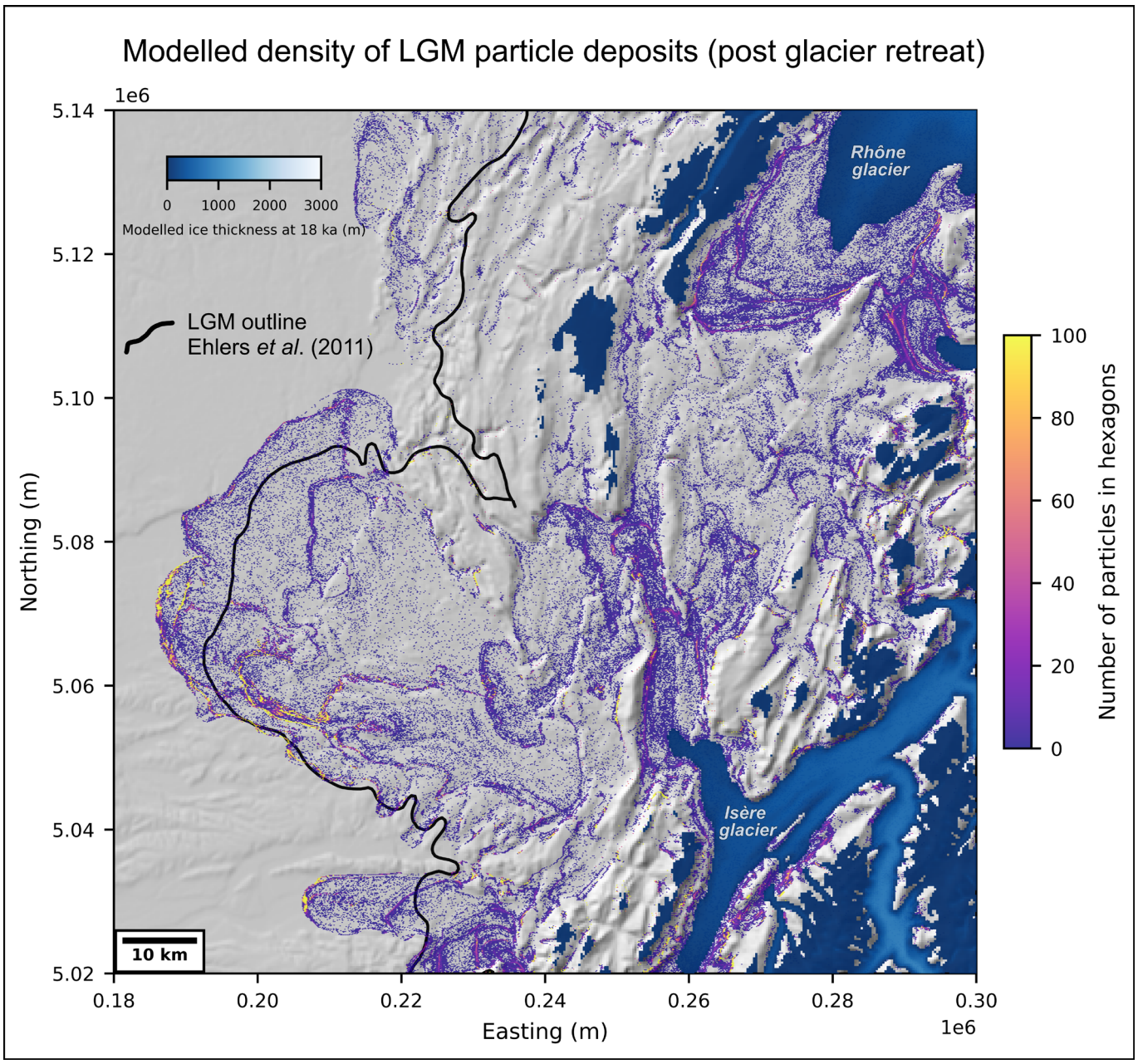

Figure S6. Map of modelled particle deposit densities at 18 ka, the final timestep of our AIF simulations of the LGM (40-18 ka), in the foreland region of the Lyon outlet glacier. See Figure S3 for the full figure caption.

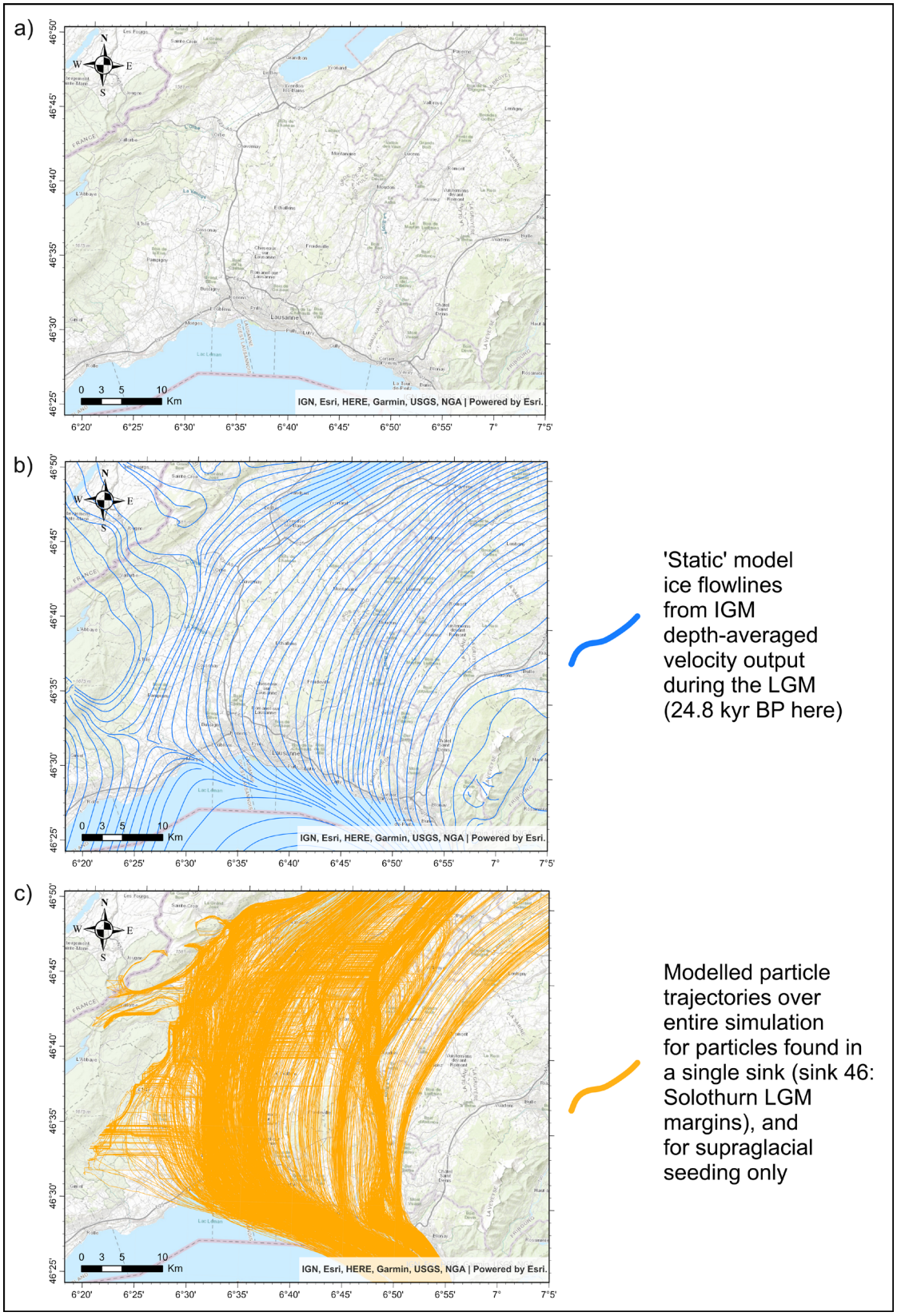

Figure S7. Maps illustrating the differences between so-called 'static' model flowlines and time-transient 3D particle trajectories, in the region of Lausanne and Yverdon-les-Bains (Vaud, Switzerland). Static flowlines (blue lines in panel b) are simply interpolated from the depth-averaged velocity field of the entire modelled AIF at a single time frame (in a post-processing manner), in this case at 24.8 ka: the timing of modelled maximum AIF volume. They only enable us to visualize the direction of ice-flow during that single model time frame. However, true ice flow directionality changes dynamically in time, as the AIF geometry evolves, and is also dependent on the height location of a specific ice entity through the ice column. 3D particle trajectories (orange lines in panel c), which we produce in this study, take into account this complexity. Here, we only show the trajectories of particles found in a single sink (sink 46).

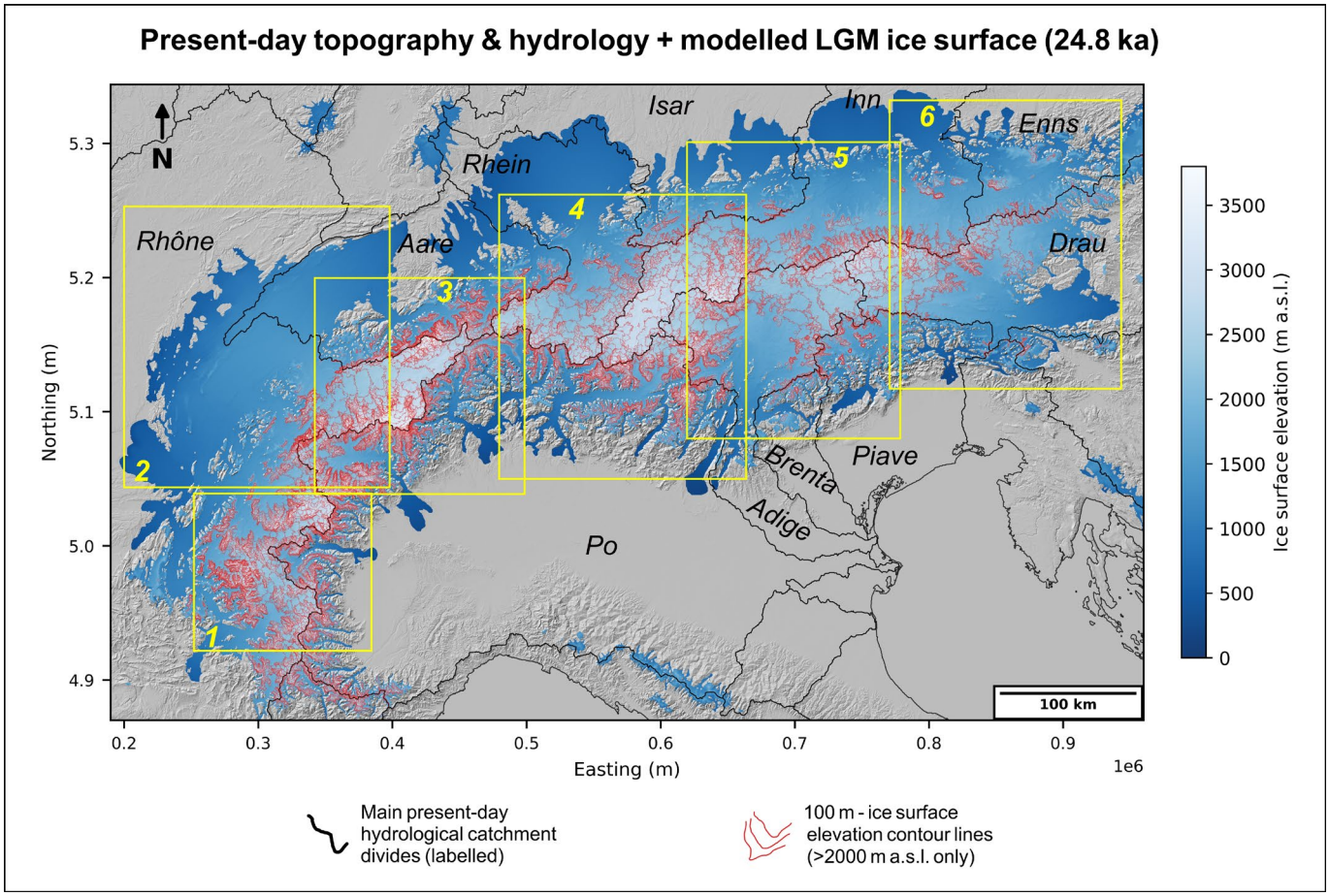

Figure S8. Map of modelled ice surface elevation during the modelled maximum LGM expansion of the Alpine Ice Field in Leger et al. (2025)'s best scoring simulation (ensemble simulation 37). This map highlights the locations of main Alpine ice domes during the LGM according to the model. It also displays the largest present-day hydrological basins in the Alps and their divides used in this study for detecting major ice transfluences when analyzing glacially transported particle trajectories crossing major hydrological divides. The yellow boxes indicate the locations of the 6 maps presented directly below; also downloadable at higher-resolution from the ice-transfluence catalogue provided in the Zenodo repository attached to this paper: https://doi.org/10.5281/zenodo.18374156.

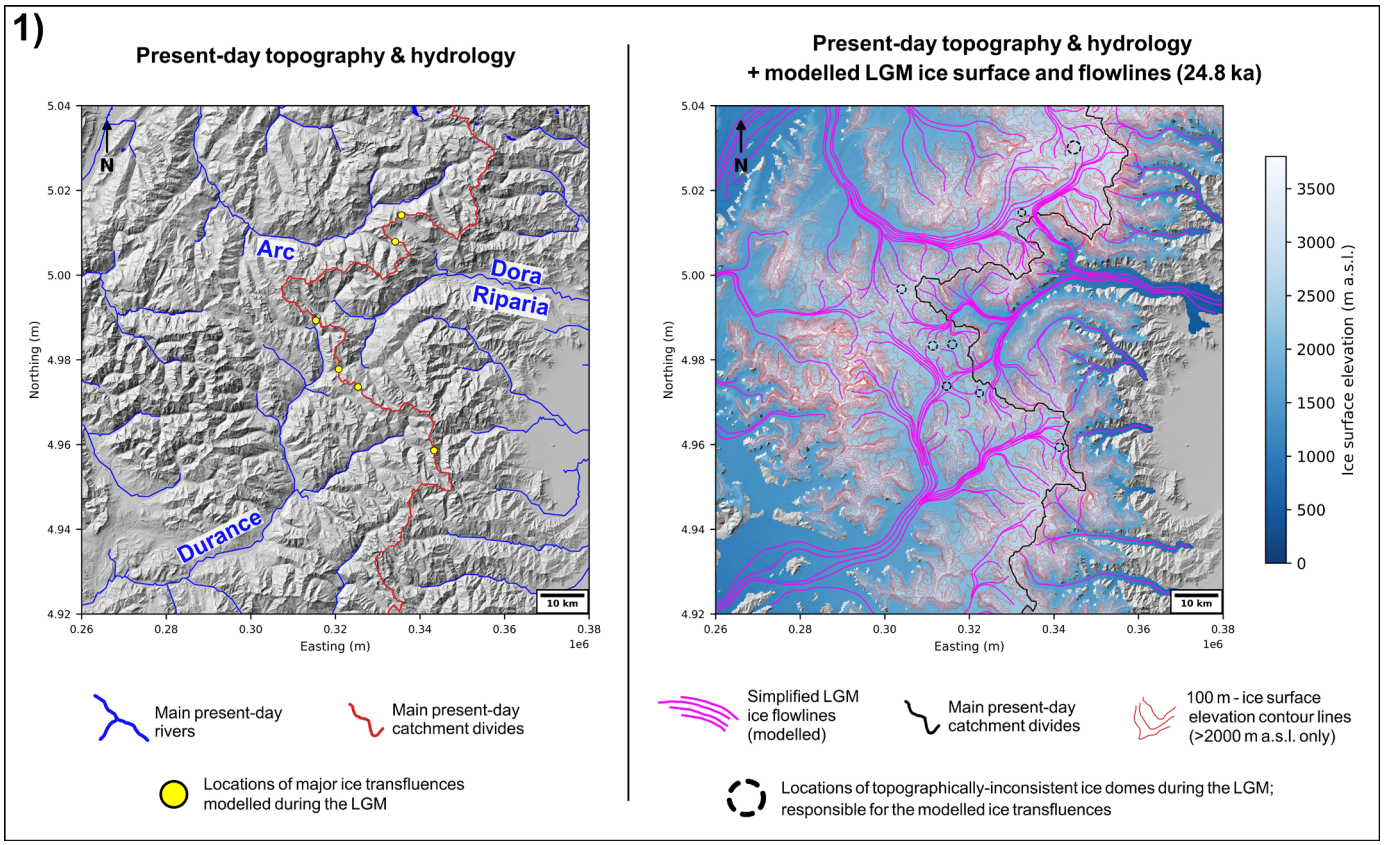

Figure S9. Map of modelled ice surface elevations and simplified 'static' ice flowlines (pink lines) during the LGM (~24.8 ka) in the southwestern region of the Alpine Ice Field, enabling to map the locations of modelled ice transfluences (yellow dots on left-hand map). These modelled transfluences can explain the complex and puzzling provenances of certain ice-contact deposits. They are here only quantified for the largest river catchments of the Alps (see Figure S8), whose divides are shown by the red line on the left-hand map, and black line on the right-hand map. Note that whilst useful for the visual purpose of this figure, the simplified glacier flowlines (pink lines) shown here are drawn from so-called 'static' flowlines, which are non-time-transient and only obtained from the depth-averaged ice velocity field modelled during the single time frame of maximum AIF volume; at 24.8 ka. These should only be considered useful in this figure to visualize the modelled flow direction of ice at the precise locations of transfluences and only during the peak of the modelled LGM. The substantially more complex and more accurate time-transient flow trajectories obtained from 3D Lagrangian particle tracking, displayed in the main paper Figs. 6, 9, for example, are more diverse but would make visualizing transfluences on a figure impossible given the large number of modelled particles and resulting cross-cutting trajectories (see Figure S7). This caption is also relevant to subsequent Figures S10-14.

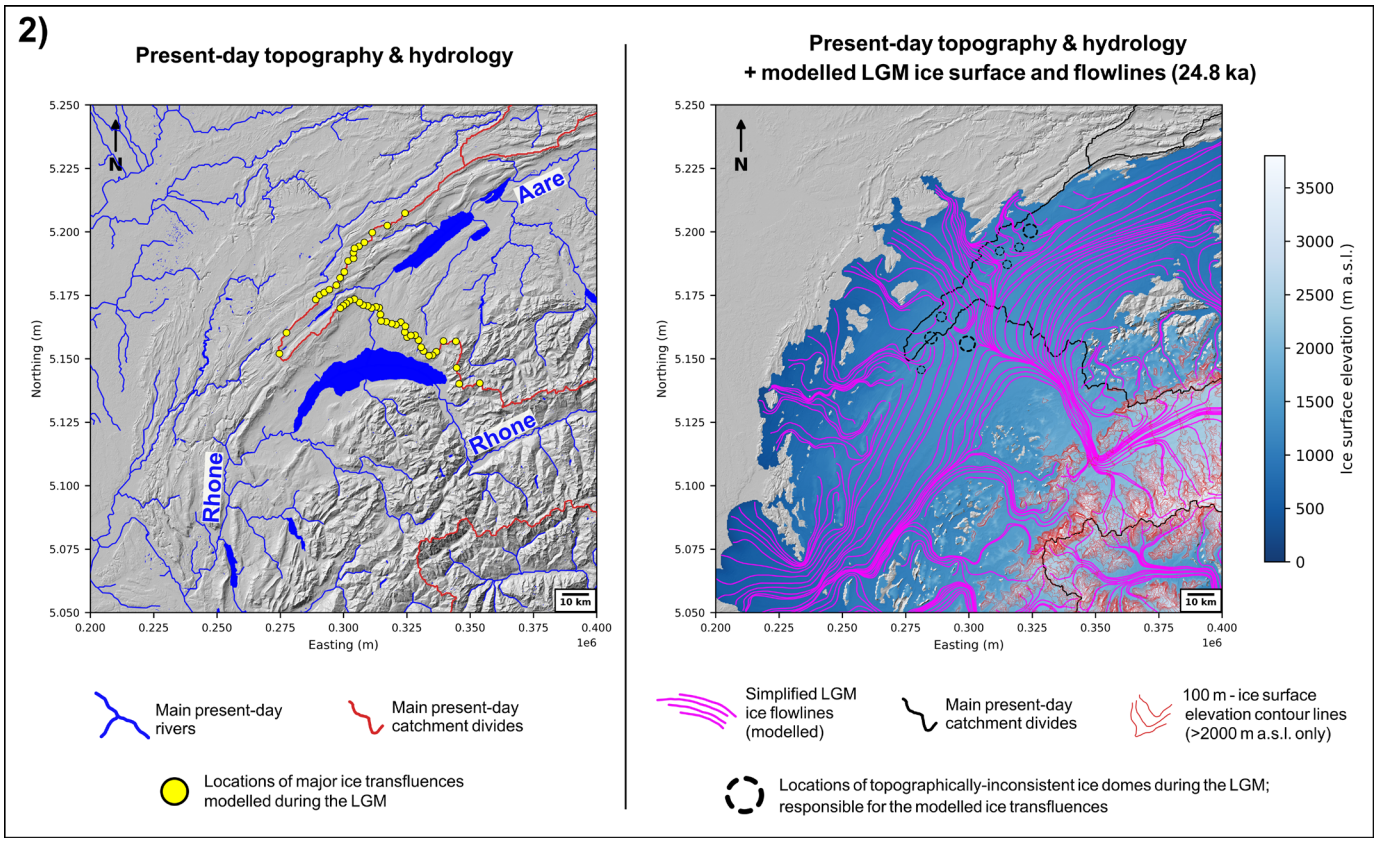

Figure S10. Map of modelled ice surface elevations and simplified 'static' ice flowlines (pink lines) during the LGM (~24.8 ka) in the Geneva Lake / Jura region of the Alpine Ice Field, enabling to map the locations of modelled ice transfluences (yellow dots on left-hand map). See Figure S9 for the full figure caption.

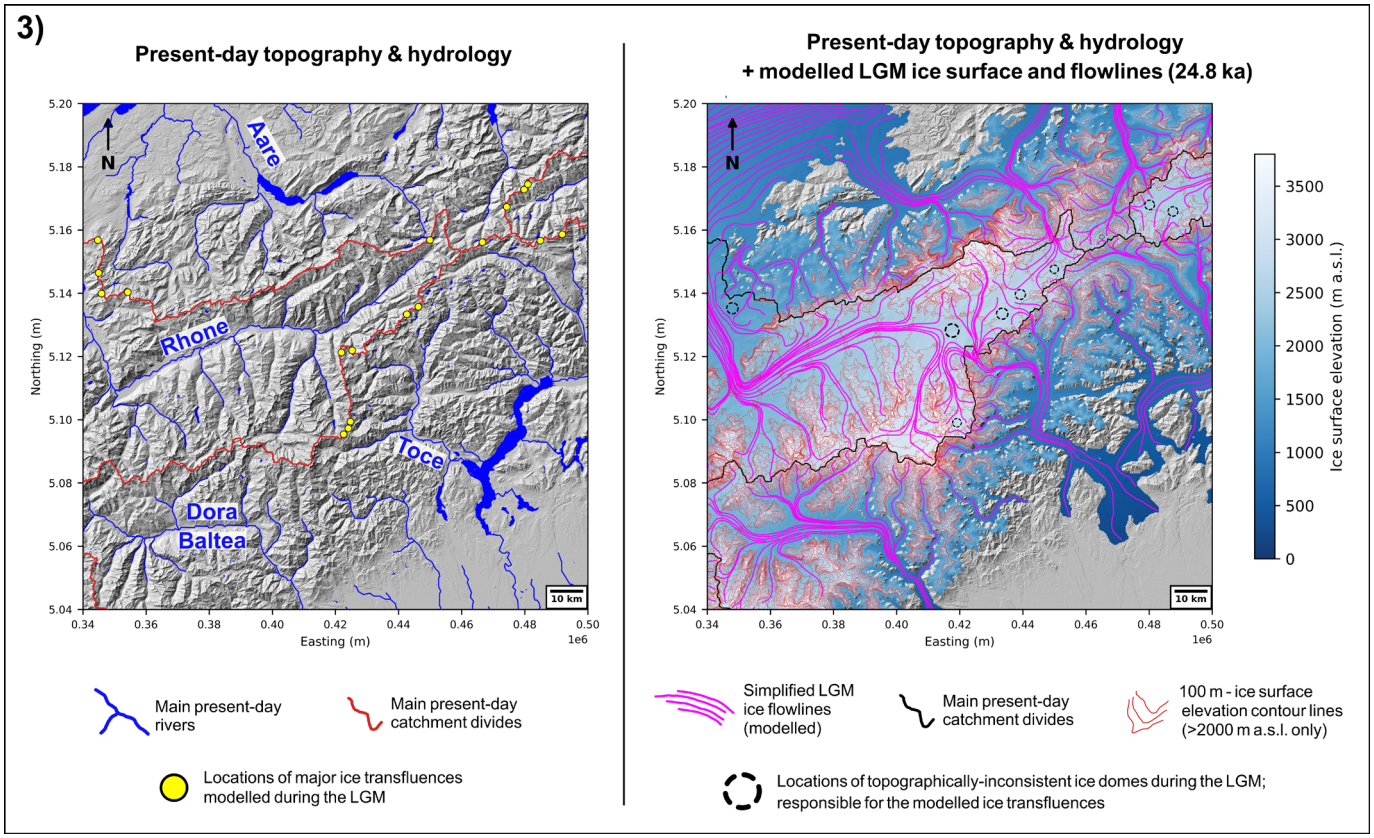

Figure S11. Map of modelled ice surface elevations and simplified 'static' ice flowlines (pink lines) during the LGM (~24.8 ka) in the region of the 'Rhône' ice dome, enabling to map the locations of modelled ice transfluences (yellow dots on left-hand map). See Figure S9 for the full figure caption.

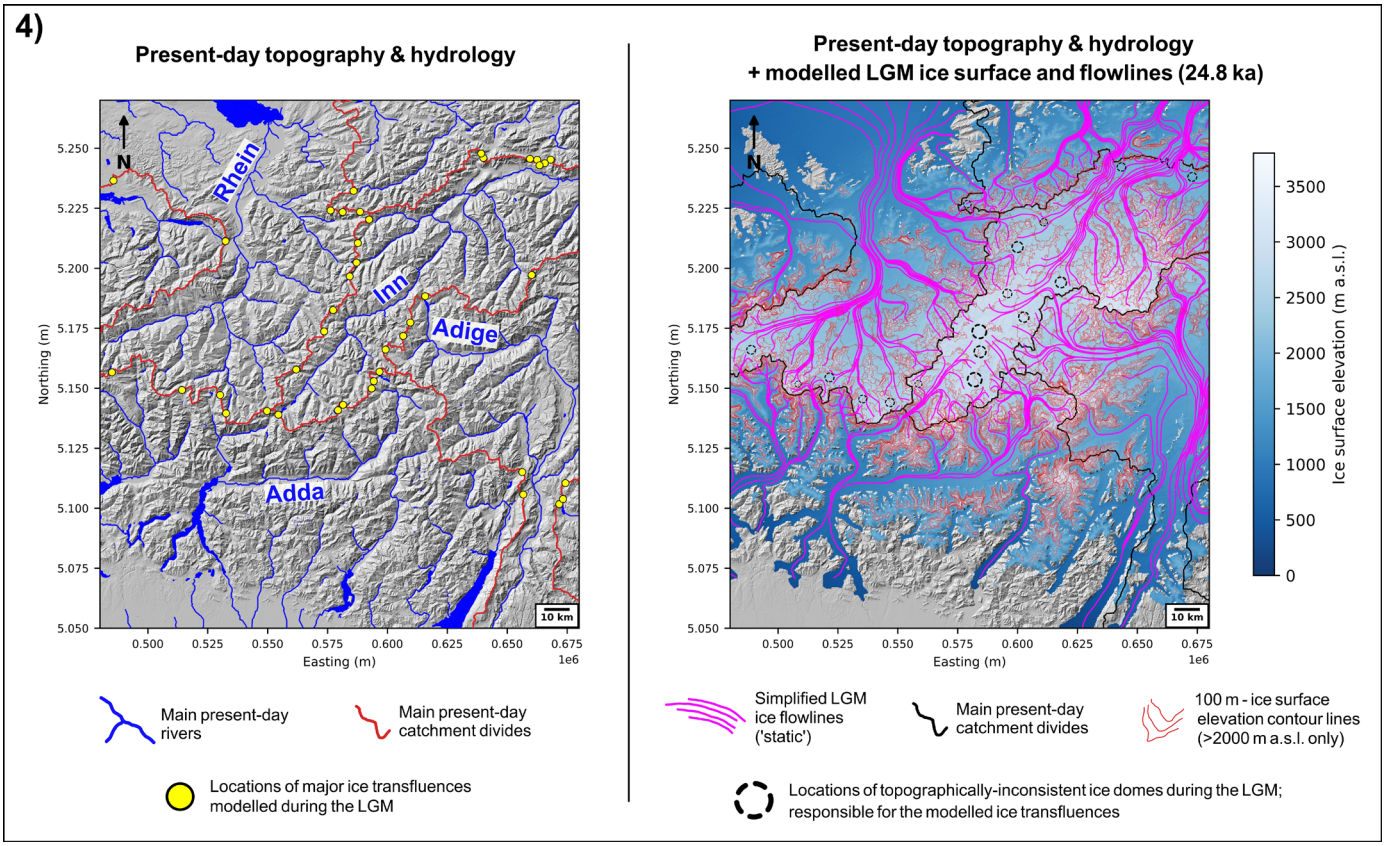

Figure S12. Map of modelled ice surface elevations and simplified 'static' ice flowlines (pink lines) during the LGM (~24.8 ka) in the region of the 'Engadin' ice dome, enabling to map the locations of modelled ice transfluences (yellow dots on left-hand map). See Figure S9 for the full figure caption.

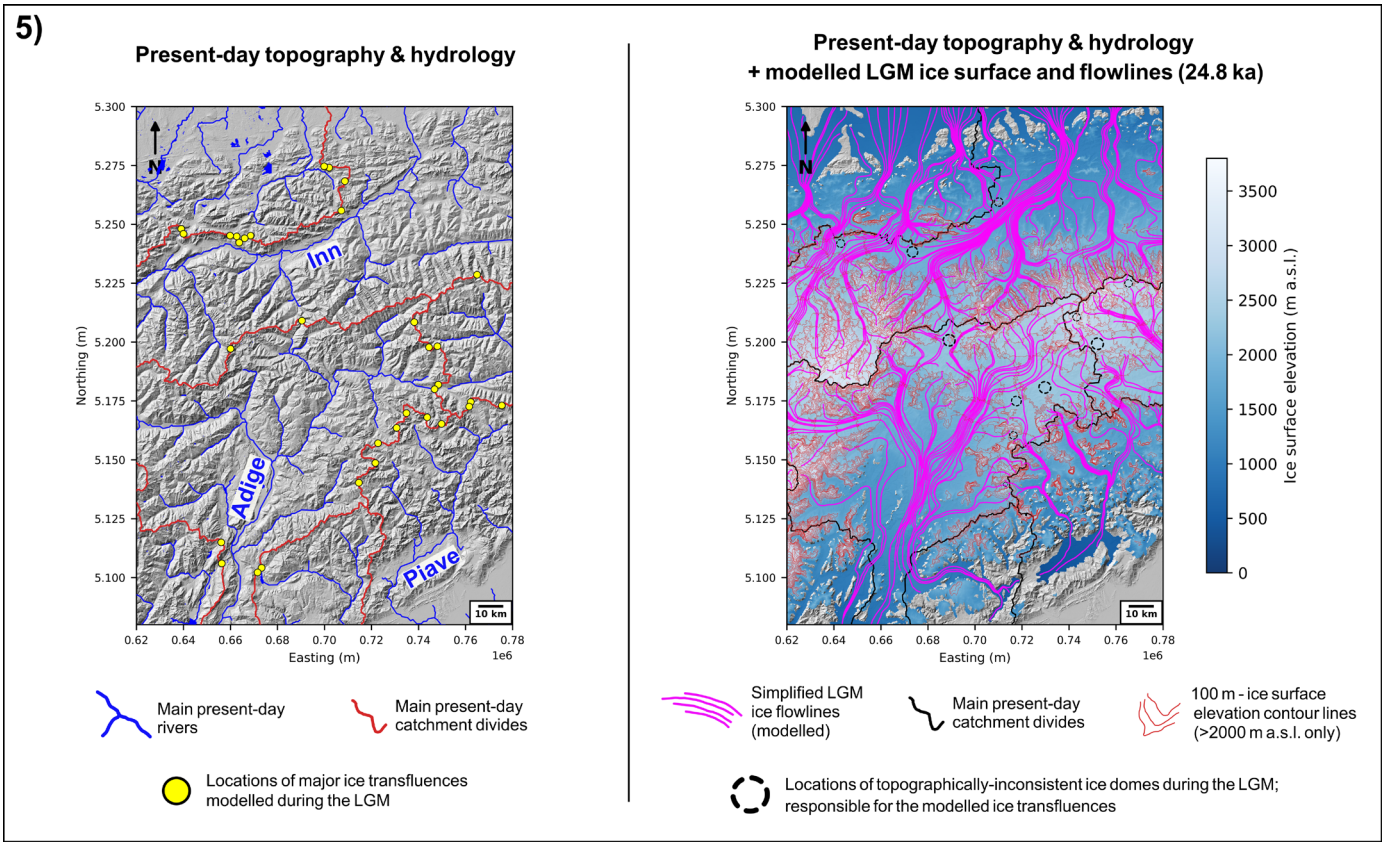

Figure S13. Map of modelled ice surface elevations and simplified 'static' ice flowlines (pink lines) during the LGM (~24.8 ka) in the region of the 'Isarco ice dome', enabling to map the locations of modelled ice transfluences (yellow dots on left-hand map). See Figure S9 for the full figure caption.

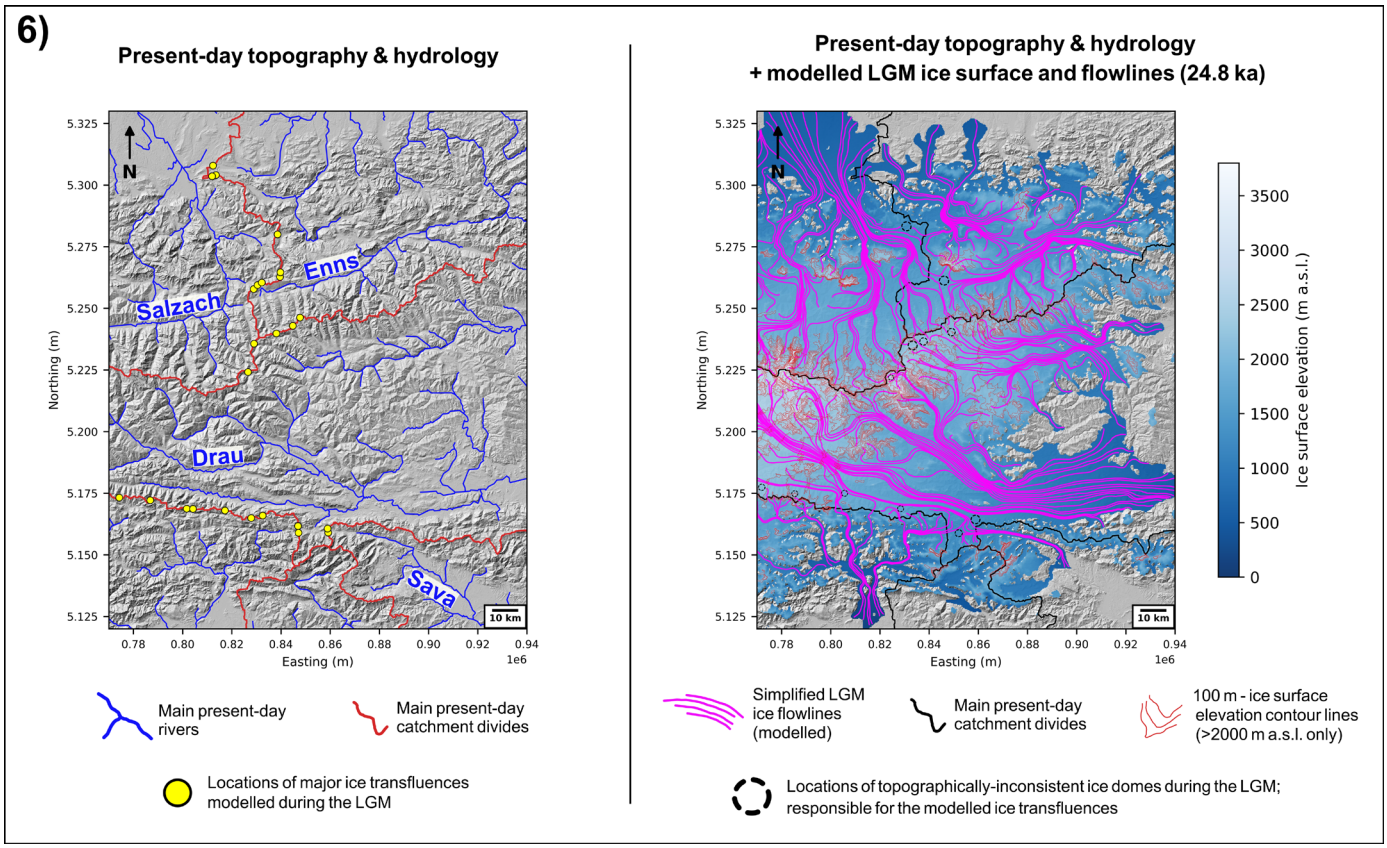

Figure S14. Map of modelled ice surface elevations and simplified 'static' ice flowlines (pink lines) during the LGM (~24.8 ka) in the easternmost region of the Alpine Ice Field, enabling to map the locations of modelled ice transfluences (yellow dots on left-hand map). See Figure S9 for the full figure caption.